Journal of Alloys and Compounds 936 (2023) 167969

Contents lists available at ScienceDirect

Journal of Alloys and Compounds

journal homepage: www.elsevier.com/locate/jalcom

Design and preparation of nickel-titanium implant for lumbar vertebra

Mahdis Parsafar [a], Sayed Khatiboleslam Sadrnezhaad [b,*], Nahid Hassanzadeh Nemati [a]

[a] Department of Biomedical Engineering, College of Medical Sciences and Technologies, Tehran Science and Research Branch, Islamic Azad University, Tehran, Islamic Republic of Iran
[b] Department of Materials Science and Engineering, Sharif University of Technology, Tehran, Islamic Republic of Iran

ARTICLE INFO

Article history:
Received 3 August 2022
Received in revised form 25 October 2022
Accepted 8 November 2022
Available online 9 November 2022

Keywords:
Implant
Nitinol
Corrosion
NiTi alloy
Bone Tissue engineering

ABSTRACT

The growing number of spine diseases and surgeries has resulted in advancements in equipment and implants. On the other hand, given the uniqueness of the anatomy of the spine, particularly in terms of mechanical characteristics, selecting the type of implant is critical. In addition to high biocompatibility and superelasticity, the implant utilized in the spine needs properties like strength, fatigue resistance, and elastic modulus close to the bone, which is found in nitinol. NiTi alloy lumbar-like samples were prepared by sintering and mechanical braiding method. The mechanical properties study revealed that the elastic modulus of the sample was 3.5 GPa, and the compressive strength at 6 % strain was 200 MPa. NiTi alloy is thermoelastic, making it a good candidate for placement in bone tissue. The biocompatibility and non-toxicity of the bone cells, with cell viability of over 4×10^4 cells within 48 h, indicate that the produced implant has suitable cellular biocompatibility. Besides, the differential scanning calorimetric test shows that the austenite start and finish temperatures are 26 and 51 °C, respectively, and martensite start and finish temperatures are − 2 and − 33 °C, respectively. These values are consistent with the body temperature of 37 °C. The corrosion test also indicates that the implant has a good corrosion resistance of about 0.3 ohm cm^2. Developing this kind of implant is intended to make treating spinal problems easier.

1. Introduction

Bone tissue engineering (BTE) has outstanding potential for regenerating bone. Bone regeneration can be stimulated by integrating osteogenic activity with a suitable synthetic extracellular matrix (ECM) [1–3]. From a chemical perspective, bioactivity, biocompatibility, and mechanical properties are three significant characteristics of substances utilized as synthetic ECM for BTE [4,5]. However, these scaffolds must also supply a porous network to permit the internal growth and angiogenesis of new bone tissue to achieve adequate integration of the substances with host tissue [6,7].

Low back pain is a severe issue for all age groups, specifically the elderly [8]. Disability-adjusted life years (DALYs) because of neck and back pains raised by 59 % between 1990 and 2015 [9], which is associated with extreme tension and an inaccurate lifestyle [10]. Treatments for back pain are difficult and costly since the backbone is a complicated system of cartilage and vertebrae that protect the spinal cord [10]. Surgical operations, including vertebral ligation and disc replacement, are suggested when noninvasive procedures have failed [11,12]. For the past 50 years, metal orthopedic devices have been applied to repair the spine shape in scoliosis [13]. Metal alloys are mainly used to make orthopedic implants that exhibit excellent mechanical properties in the field [14,15]. Also, stainless steel has been applied to correct the backbone for a long time [16]. Lately, nitinol has drawn much concentration owing to its outstanding characteristics [12,17,18]. NiTi alloys are known to have excellent mechanical properties [19]. In addition to its shape-memory characteristics, it also attracts concentration as a biomaterial for clinical use [20,21]. Specifically, NiTi alloy foam represents a new category of biomaterials that offers a superior combination of low density and functional features, including adjustable elastic modulus and internal growth capacity of new bone tissue [22,23]. These benefits make titanium nickel alloy an encouraging substance for bone tissue regeneration.

Making a metal implant for the lumbar vertebra that provides unique properties (including shock absorption and appropriate mechanical properties) in the vertebral region has been one of the gaps in orthopedic medical engineering. In addition to the simplicity of the forming process, the use of NiTi is also biocompatible and economical. Therefore, this alloy is considered the most appropriate option for the above purpose. In this study, a NiTi implant was prepared by the sintering and braiding method as a lumbar vertebra.

* Corresponding author.
E-mail address: sadrnezh@yahoo.com (S.K. Sadrnezhaad).

https://doi.org/10.1016/j.jallcom.2022.167969
0925-8388/

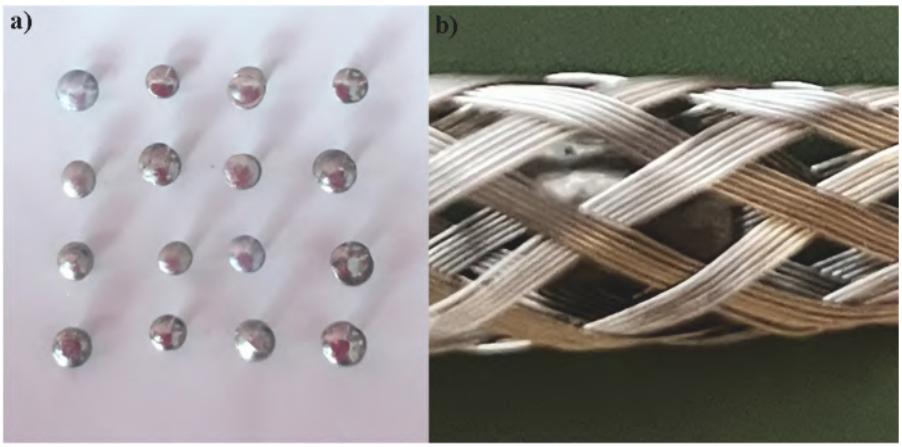

Fig. 1. Images of prepared samples: a) sample without braided cover (sample 1), and b) sample with braided cover (sample 2).

Its biocompatibility and mechanical properties were then determined. So far, no research has been done on the use of nitinol alloy as a lumbar vertebra based on the patient's anatomy and the characteristics considered by the researchers of this study. The technique of sintering and braiding, while being simple and affordable, is new and helpful in creating this wanted piece.

2. Materials and methods

2.1. Preparation process

Titanium hydride (99.5 % purity, ≤50 μm), Ni powder (99.9 % purity, ≤ 10 μm), and urea (99.5 % purity) were purchased from Merck. Nitinol wire (diameter = 0.25 mm) was obtained from Baoji Hanz Company. In this research, the nitinol metal powders were mixed with urea as a space holder material to create 50 % porosity and a nominal Ti–50.0 at % Ni, and then pressed with a pressure of 150 MPa. The ratio of Ti: Ni: Urea was 1:1:1. The urea diameter was selected to be 100–600 μm. Then, it was transferred to the furnace with an argon atmosphere at 1050 °C for 2 h to carry out the sintering operation. It is worth noting that the burning of urea was done at 200 °C after 1 h, and the decomposition of titanium hydride was also done at 500 °C after 1 h. The sample obtained had a diameter of 5 mm and a height of 7 mm (sample 1). Nitinol wires with a diameter of 0.25 mm were braided around sample 1. The product was called sample 2. A braiding machine aided in doing the job. A pattern was created and braided, then it was placed around the sample's circumference in the shape of a cylinder according to the sample's dimensions. Fig. 1a and b show the images of prepared samples. The

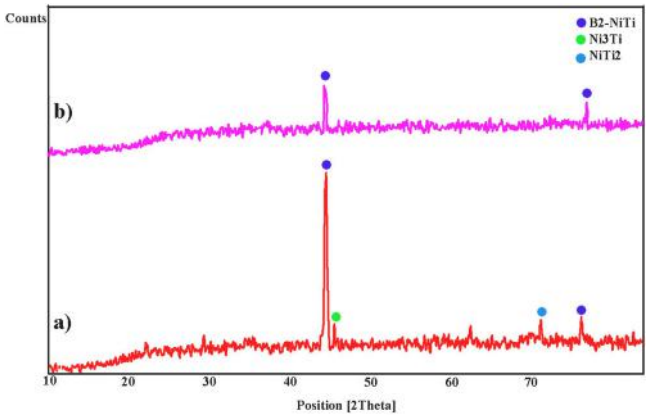

Fig. 2. XRD patterns of a) porous nitinol sample (sample 1) and b) nitinol wire.

braiding machine has six spools, each connected to a wire. The wires connected to the spools wrap around the polymer cylinder in an upside-down pattern, and finally, we removed the braided piece from the cylinder.

2.2. Physical instruments

An XRD diffractometer (SEIFERT PTS 3003) was applied to confirm the alloying procedure and examine the phase structure of the alloy by CuKα radiation (λ = 1.54). A scanning electron microscope (LEO440i) was used to observe the porous structure of NiTi alloy. Loading and unloading compression experiments were performed at 25 °C to examine the shape memory characteristic of NiTi alloy, utilizing cylindrical pieces with a height of 15 mm and a diameter of 10 mm (STM-50). The nominal strain rate was 1.0×10^{-5} s^{-1}. The corrosion behavior was assessed using a potentiodynamic polarization test with an EG&G Model 273 A potentiostat operating between − 0.5 V and 2.2 V and a 1 mV/S scanning rate.

2.3. MTT assay and cell adhesion

The in vitro biocompatibility of nitinol was studied by the MTT assay. Human osteosarcoma MG63 cells with the code (NCBI C 555) were obtained from the National Cell Bank of Iran, Pasteur Institute of Iran. MG63 cells were cultured with 85 % humidity in an incubator at 37 °C and 5 % carbon dioxide in RPMI-1640 medium comprising 50 μg of streptomycin and 50 units of penicillin per mL of culture medium supplemented with 10 % fetal bovine serum (FBS). The cells are extracted from the surface of the flask by trypsin (0.25 %) after 3–4 days (formation of cell layer), and a suspension containing 4×10^4 cells per mL is made ready for use. Besides, the specimens were oven-sterilized (dry heat) and set in separate wells of a 12-well microplate, with one well left empty as a control. After putting them in an incubator, add 2 mL of cell suspension into each well. The wells were then filled with the MTT solution and incubated again. (50 mg of MTT powder was dissolved in 10 mg of PBS (150 mM) to provide an MTT solution at a 5 mg/mL concentration). The cell supernatant was withdrawn after 3–5 h of incubation at 5 °C. Then, the respective wells were filled with 1 μL of isopropanol solution. The related plate chambers were shaken for 1–4 min. A microtiter of 2 nm was then used to read their contents [24].

The braided nitinol was immersed in the SBF for 14 days at 37 °C to determine its bioactive behavior. The protein-free and acellular SBF was prepared according to Kokopo's recipe [25]. The prepared SBF was buffered to pH 7.4 at 37 °C by adding 1 M Hydrochloric acid and Tris (hydroxymethyl aminomethane).

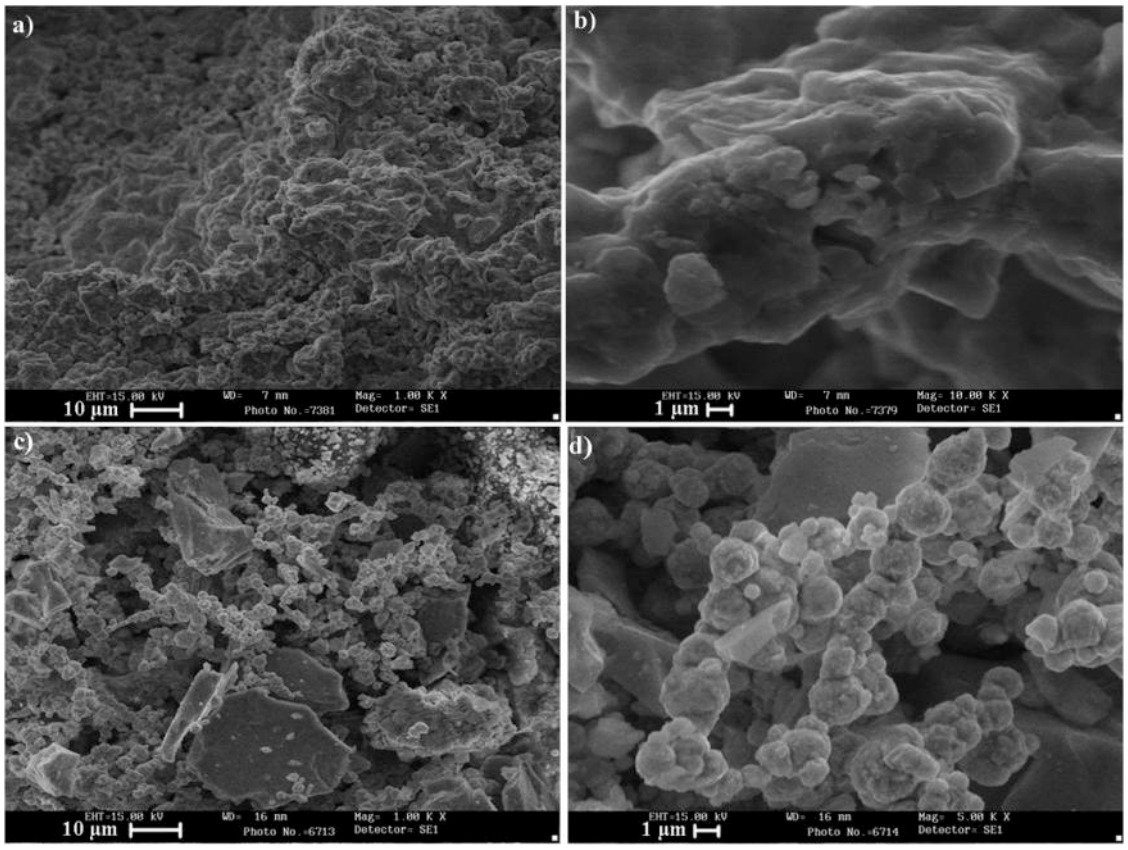

Fig. 3. SEM images of samples (a and b) without braided cover and (c and d) with braided cover in two different scales.

Table 1
Potentiodynamic polarization test results of as-prepared samples.

Sample	Corrosion resistance (ohm cm^2)	Corrosion potential (V)
With braided cover	0.33	-410
Without braided cover	0.31	-390
Nitinol wire	0.53	-616

Table 2
Porosity percentages obtained from porosity test.

Open porosity (%)	Closed porosity (%)	Total porosity (%)
44	7	51

MG63 cells are human and obtained from sarcoma disease. It also has the morphology of fibroblast and bone tissue. DMEM culture medium (Gibco) containing 10 % FBS (SeroMed), 100 IU/mL penicillin, and 100 µg/mL streptomycin (Sigma) was used to prepare osteogenic cells. A scanning electron microscope (LEO440i) was used to determine the morphology of the cultured cells on the samples. For this purpose, first, the samples were sterilized in an autoclave and placed in a 96-well microplate for cultivation. The samples were incubated in the presence of DMEM and MG63 cells at 37 °C for 32 h. Following incubation, the samples were washed in PBS and fixed with a 0.25 % glutaraldehyde solution at 4 °C for 2 h, repeatedly [26]. The cultivated surfaces were then gradually dewatered and lyophilized using ethanol. The samples were coated with Au for FESEM analyses.

2.4. Corrosion behavior

The corrosion behavior of samples was evaluated since implants in the body degrade when exposed to human fluids. The samples were put in PBS solution for this purpose. The corrosion behavior was assessed after immersion in the simulated solution. In this test, a three-electrode cell was used, where platinum was used as the counter electrode, saturated calomel as the reference electrode, and the sample as the working electrode. The data were analyzed with Corview software. Corrosion potential and corrosion current density (i_{corr}) were calculated from the intersection of the tangents drawn on the anodic and cathodic parts of the polarization curves using the linear polarization method. Therefore, the corrosion current, corrosion potential, and corrosion resistance can be identified in this way that the polarization resistance (R_p) is calculated using the Stern-Gray equation:

$$R_p = \frac{\beta_a \beta_c}{2.03(\beta_a + \beta_c)i} \quad (1)$$

β_a and β_c are the anodic and cathodic Tafel slopes in the curve, respectively.

2.5. Porosity test

Archimedes' principle was used to check and prove the porosity of the samples, and the percentage of porosity was calculated using the following formulas:

$$D_b = \frac{W_a}{W_e - W_b} Dl \quad (2)$$

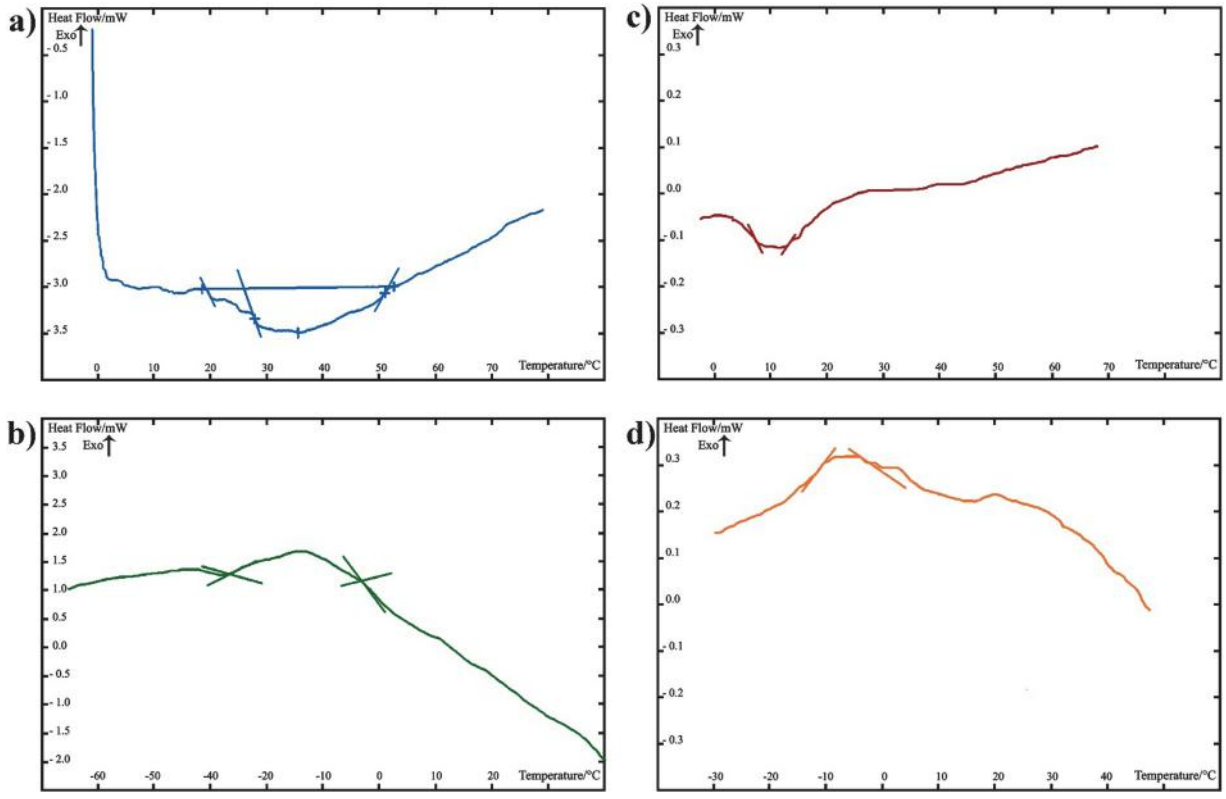

Fig. 4. DSC heating and cooling curves of (a, b) sample with braided cover, and (c, d) nitinol wire.

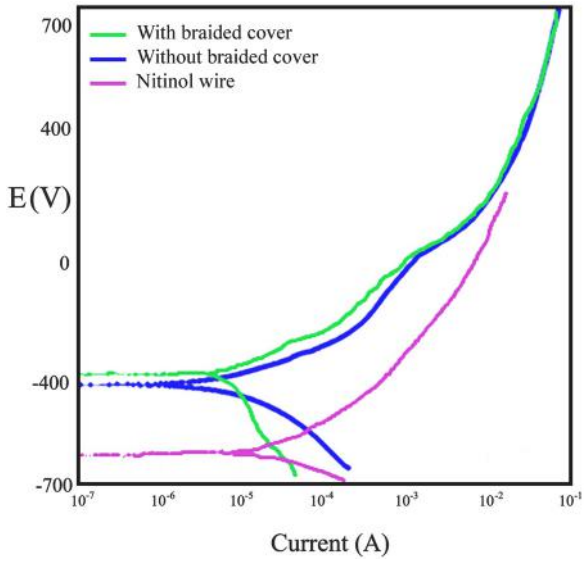

Fig. 5. Dynamic potential polarization diagram of samples with and without braided cover and nitinol wire.

$$D_{as} = \frac{W_a}{W_a - W_b} Dl \tag{3}$$

$$P_t = 100 \quad X \quad (1 - \frac{D_b}{D_t}) \tag{4}$$

$$P_a = 100 \quad X \quad (1 - \frac{D_b}{D_{as}}) \tag{5}$$

$$P_c = P_t - P_a \tag{6}$$

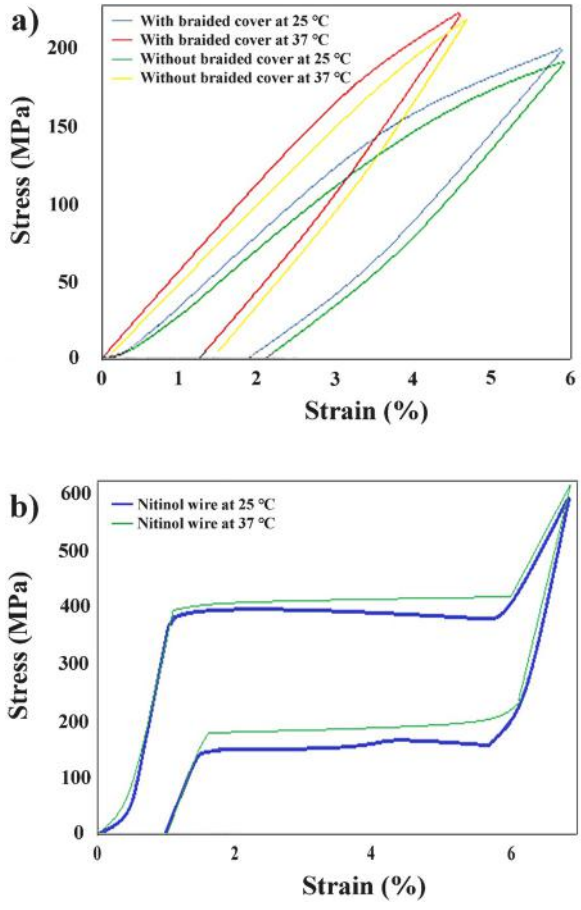

Fig. 6. Stress–strain curves of loading–unloading compressive tests of (a) samples with and without braided cover and (b) nitinol wire at 25 and 37 °C.

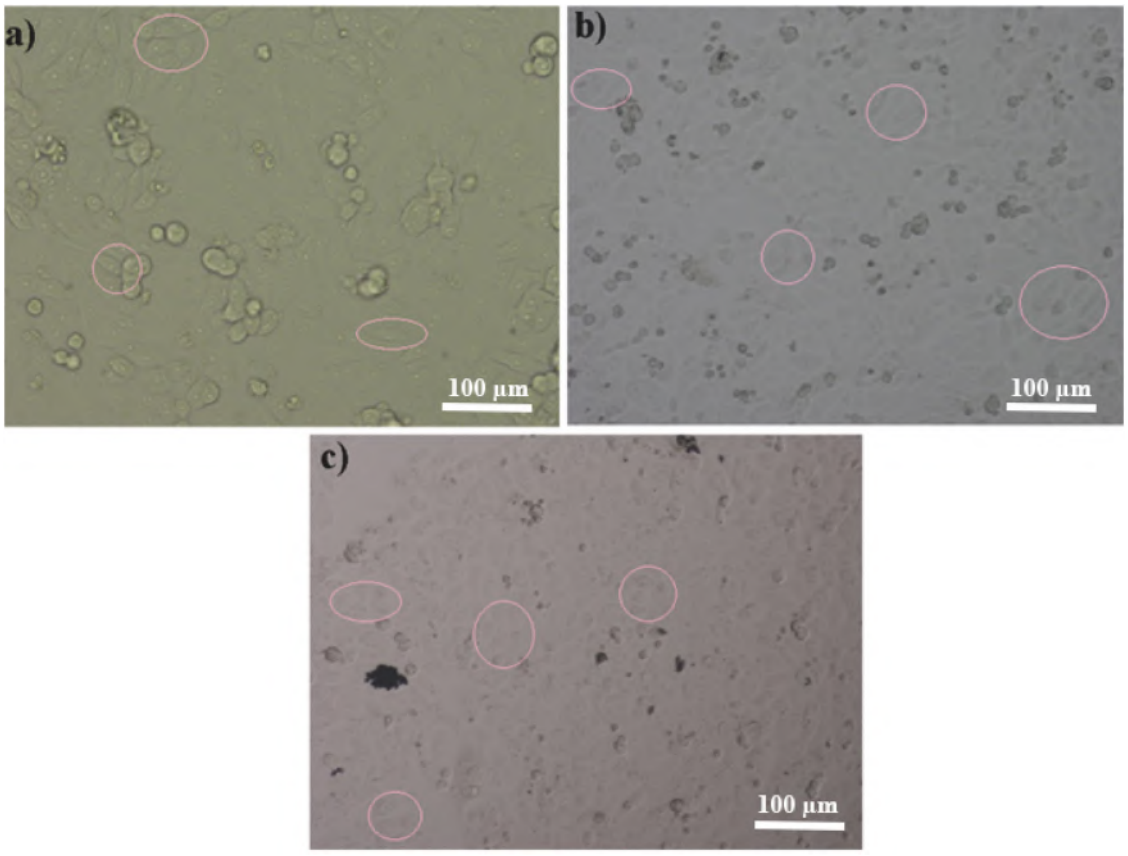

Fig. 7. Optical microscope images of cell growth of (a) control, (b) sample 1 (without braided cover), (c) sample 2 (with braided cover). The red circles are a selection of cells.

D_b is bulk density, D_{as} is bulk density of solid, Pt is total porosity, P_a and P_c is open and closed porosity percentage, respectively. D_t is the theoretical density of the nitinol alloy, which is calculated to be 6.44 g/cm^3, W_a is the sample's dry weight, W_e is its wet weight, and W_b is its immersion weight. Dl is the density of water [27].

3. Results and discussion

3.1. XRD results

Fig. 2 displays the porous sample (a) and nitinol wire (b) XRD patterns. B2-NiTi is the predominant phase in the porous sample, and the sample also contains a small amount of Ni_3Ti and $NiTi_2$. During the annealing process, the following reactions occur:

$$TiH_2 + 3Ni \rightarrow H_2 + Ni_3Ti + Q \quad (7)$$

$$2TiH_2 + Ni \rightarrow 2H_2 + NiTi_2 + Q \quad (8)$$

$$TiH_2 + Ni \rightarrow H_2 + NiTi + Q \quad (9)$$

Ni_3Ti and $NiTi_2$ are stable substances in the NiTi binary system. The movement of nickel and titanium atoms towards each other causes the formation of the $NiTi_2$ phase in titanium-rich areas and the Ni_3Ti phase in nickel-rich areas. Furthermore, reactions (8) and (9) are more thermodynamically possible. According to the Ni-Ti equilibrium diagram, three intermediate phases can exist; Ni_3Ti, which melts congruently near 1653 K and has a hexagonal closed-packed superlattice structure; NiTi, which melts congruently near 1583 K and has a CsCl-type structure at elevated temperatures; and $NiTi_2$, which melts peritectically near 1257 K and has a complex $E9_3$ cubic-type structure with 96 atoms per unit cell [28,29]. As a result, preventing the formation of these phases during the sintering process is difficult, and they usually exist in the structure of the sintered parts. Additionally, the sample's porosity limits the penetration of nickel and titanium elements. This limitation causes the increase of titanium-rich and nickel-rich areas and the formation of Ni_3Ti and $NiTi_2$. According to the X-ray diffraction pattern, the sample has an austenitic structure. This construction is due to the enrichment of samples with nickel. Increasing the percentage of nickel decreases the starting temperature of the martensite phase [30]. The cubic nitinol structure B2 is located above the austenite finish temperature. Rhombohedral, tetragonal, orthorhombic, and monoclinic structures exist below this temperature [31,32]. Meanwhile, BCC/rhombohedral structural modifications give Ni-rich NiTi its distinct memory characteristics [33]. As a result, the samples have an austenitic structure at room temperature. In addition, Fig. 1b, which is specific to Nitinol wire, shows that this wire has only an austenitic phase.

3.2. Morphology study

Fig. 3 depicts the SEM images of the sample without and with a braided cover, showing that the desired mixing and porosities have occurred. Both samples have an as-cast structure, indicating melting during the preparation process and consisting of NiTi matrix and primary Ti2Ni phase. The existing pores indicate the areas where the space holder was present, and after exposure to high temperatures, it evaporated and left space. The presence of porosity is one of the requirements of metal implant fabrication to prevent the stress shield phenomenon and to bring the modulus closer to the bone

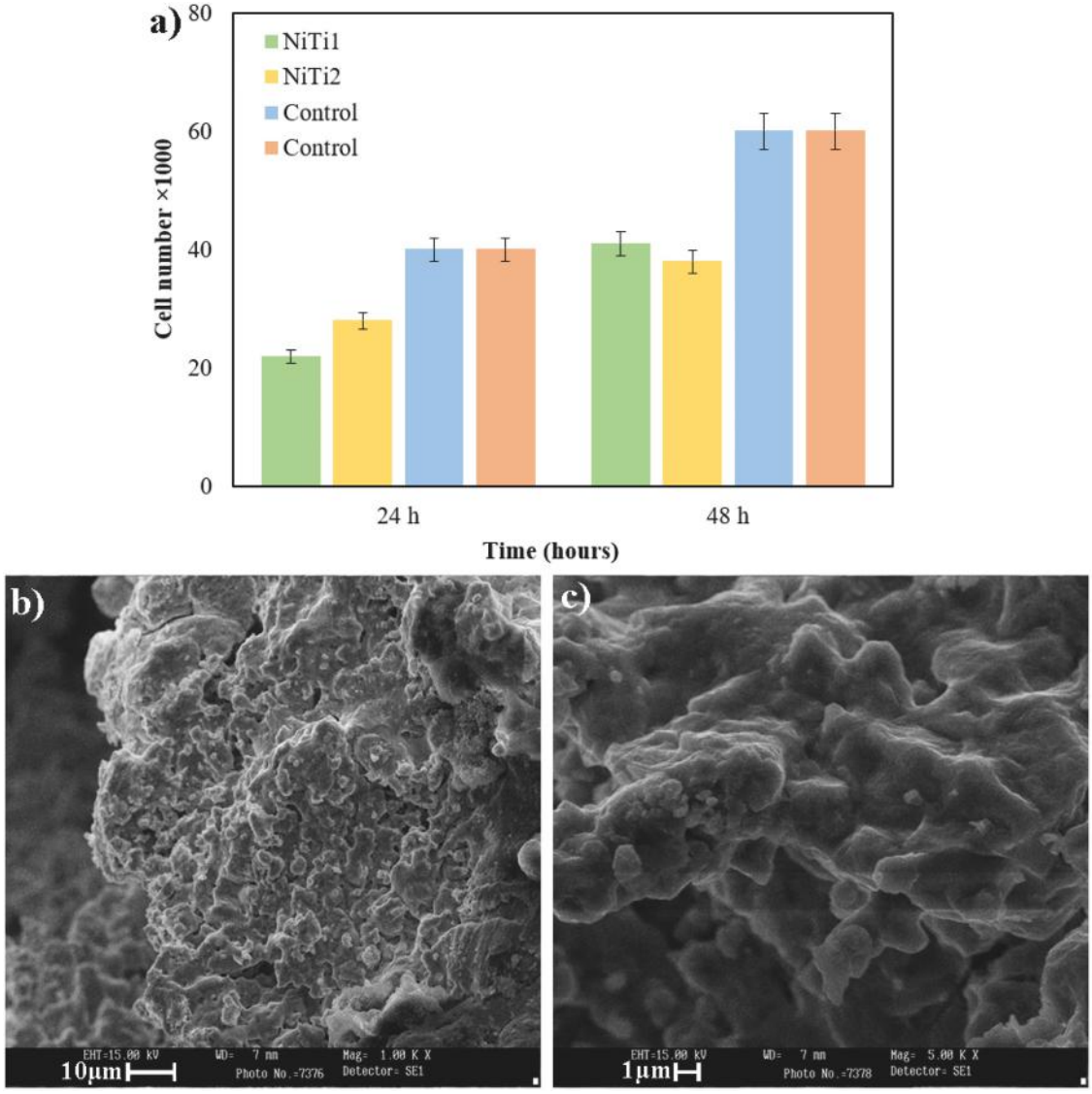

Fig. 8. (a) MTT results of sample 1 (without braided cover), and sample 2 (with braided cover), (b, c) SEM images of cell-cultured of sample 2.

modulus by creating porosity. The connection of the pores to each other, indicating the open pores, is another case. Most pores must be open to plant an implant in the body, and expect biocompatibility, bioactivity, good bone connection, and fluid and cell penetration. On the other hand, the excellent cohesion and compression of the implant can be seen as a result of cold pressing.

Open pores are those that can exit the sample, whereas closed pores are those that are located separately within the substance. Open pores are suitable for medical applications [32,34]. These pores allow cells to be absorbed into the implant, resulting in better implant-body integration. Table 2 depicts the porosity of the samples. The sample has 44 % open pores and 7 % closed pores. The porosity should be between 35 % and 80 % to improve biocompatibility and connect the implant to the bone. Given that the current sample has 51 % porosity, it has good biocompatibility properties, and its mechanical properties do not deteriorate [35].

3.3. DSC measurement

The phase change of austenite to martensite occurs when the nitinol alloy temperature is reduced, and the transformation of martensite to austenite happens in the heating mode [36,37]. The differential scanning calorimeter method is used to identify the start and finish temperatures of the transformations. Fig. 4 unveils the DSC graphs during the heating and cooling cycles of the braided cover sample. According to the DSC test results of the braided cover sample, the start temperature of the austenite phase (A_s) is 26 °C, the finish temperature of the austenite phase (A_f) is 51 °C, as well as the start (M_s) and finish (M_f) temperatures of the martensite phase are − 2 °C and 33 °C, respectively. Additionally, the DSC test result (Fig. 4) for Nitinol wire reveals that the austenite phase's start and finish temperatures are 5 and 15 °C, respectively, and the martensite phase's start and finish temperatures are − 10 and 0 °C, respectively. The nitinol piece should be kept below − 33 °C by applying a little mechanical pressure to reduce the sample's diameter (600 µm). After the implant enters the body and is placed in the target area, it reaches its austenite temperature and expands by about 4 %. This 500–600 µm opening simplifies surgical conditions and provides a platform for optimal implant placement.

3.4. Corrosion study

Potentiodynamic polarization test determined the corrosion behavior of metals. Fig. 5a depicts the test results for the prepared

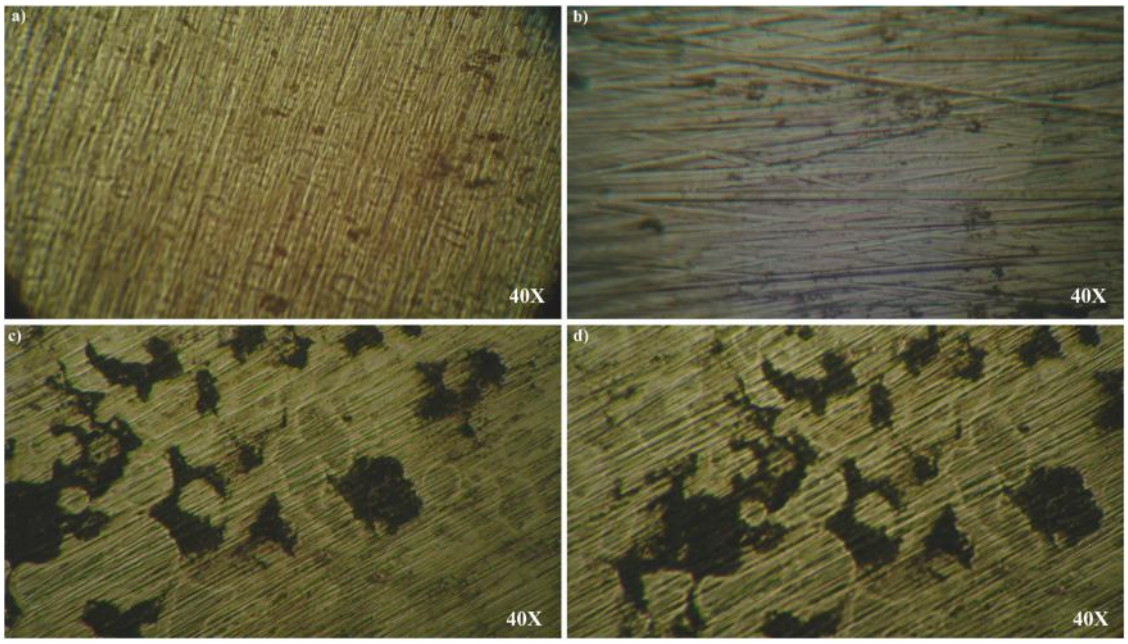

Fig. 9. The optical microscopy images of braided cover sample before (a and b), and after (C and d) immersion in SBF.

samples. As listed in Table 1, the corrosion resistance of the sample with and without braided cover and nitinol wire are 0.33, 0.31, and 0.53 ohm.cm$_{2,}$ respectively, and the corrosion potential of the sample with and without braided cover and nitinol wire are − 410, − 390, and − 616 V, respectively. The results demonstrate the similarity of the corrosion properties of the sample with and without a braided cover. Fig. 5b reveals the corrosion diagram of nitinol wire. These values indicate that the implant piece has good corrosion resistance and is suitable for body conditions [38].

3.5. Compressive mechanical properties test

The compressive mechanical properties test was carried out for the samples with and without a braided cover, at 25 and 37 °C, up to a strain of 6 %, to examine the sample's mechanical characteristics [39]. The outcome is depicted in Fig. 6a and b. The diagram shows that the residual strain in both samples with and without a braided cover is about 2 %, and the elastic strain is about 4 %. These findings demonstrate the fabricated implant's thermoplastic nature and point out this value's similarity across both investigational modalities. It can be deduced that the sample with a braided cover has higher superelastic qualities by noting that the residual strain is less than 0.2 % when it has a braided cover. The elastic modulus of the samples is 3.5 GPa, and the compressive strength at 6 % strain is 200 MPa. The mechanical properties of the sample are similar to those of cortical bone.

3.6. MTT assay

The microscopic photographs obtained from the cytotoxicity test are shown in Fig. 7(a-c). The cells had good growth and proliferation on nitinol samples with and without braided cover. Samples 1 and 2 are related to nitinol pieces without and with braided covers, respectively, which both had good growth and proliferation. It demonstrates that braiding does not result in cytotoxicity. By examining the images of samples 1 and 2 and comparing them to the MTT test, it is clear that the number of cells has not only decreased but also increased, indicating cell growth. The highlighted areas in the figures are excerpts from the presence of cells. The MTT test was performed on samples 1 and 2 (Fig. 8a). The diagram displays the number of cells in 24 and 48 h. By examining the graph and comparing the cell viability of the nitinol samples and the controls, it can be concluded that in addition to the nitinol sample having little toxicity and the cell viability on it being suitable, the sample with the braided cover does not cause cell death and the cell survival rate is almost the same as the sample without the braided cover.

The SEM images of the samples after cell culture (Fig. 8b and c) reveal that the cells did not adhere to the surface, but the MTT and the cytotoxicity tests indicated good cell adhesion. There may be several explanations for why cell adhesion was not visible in these images. i) It took a while for the cells to stabilize in the sample and be photographed. ii) There is a possibility of operator error in placing the sample under the microscope, which causes the cell adhesion layer to be torn off due to mechanical pressure. iii) The SEM microscope used is a LEO440i model and has a sticky part for fixing the sample, which can cause the cell layer fixed on it to tear off.

The surface morphology of a braided NiTi alloy before and after immersion in SBF is shown in Fig. 9. Before immersion, this sample has a very smooth surface (Fig. 9a and b). The island structure has formed after 14 days of immersion in SBF, and many tiny granular particles have grown on the surface (Fig. 9c and d). The nucleation of these precipitates preferentially takes place on the island. As the immersion time increases, so does the quantity and size of these precipitates. Fig. 9c and d show that the sediments are composed of many small crystallites.

4. Conclusions

In this research, the lumbar vertebra implant piece with a braided cover was created by the mechanical alloying process. The effect of this cover was investigated on the properties of the piece. According to the X-ray diffraction pattern, NiTi alloy has an austenitic structure. Porosity test results show that the NiTi has 50 % porosity and good biocompatibility properties. The MTT results showed that the samples were not harmful to the cells and increased cell proliferation while retaining a respectable level of cell viability. According to the DSC test results, the martensite phase's start (M_s) and finish (M_f) temperatures were − 2 °C and − 33 °C, respectively. The austenite phase's start (A_s) and finish (A_f) temperatures were

26 °C and 51 °C, respectively. The mechanical properties study revealed that the elastic modulus of the sample was 3.5 GPa, and the compressive strength at 6 % strain was 200 MPa. The mechanical properties of the samples are similar to cancellous bone.

CRediT authorship contribution statement

Mahdis Parsafar: Research & Investigation, Data curation, Analysis, Writing – original draft, **Sayed Khatiboleslam Sadrnezhaad:** Idea & Conceptualization, Project administration, Supervision, Writing – review & editing. **Nahid Hassanzadeh Nemati:** Project administration, Supervision, Verification,

Data Availability

No data was used for the research described in the article.

Declaration of Competing Interest

The authors declare that they have no known competing financial interests or personal relationships that could have appeared to influence the work reported in this paper.

Acknowledgments

The authors appreciate the general support of Iran National Science Foundation, Islamic Republic of Iran (INSF).

References

[1] T.L. Livingston, Bioactive Scaffold for Bone Tissue Engineering: An in Vivo Study, University of Pennsylvania, 1999.
[2] Y. Su, M.S. Toftdal, A. Le Friec, M. Dong, X. Han, M. Chen, 3D electrospun synthetic extracellular matrix for tissue regeneration, Small Sci. 1 (2021) 2100003.
[3] M. Ghanbari, M. Salavati-Niasari, F. Mohandes, B. Dolatyar, B. Zeynali, In vitro study of alginate–gelatin scaffolds incorporated with silica NPs as injectable, biodegradable hydrogels, RSC Adv. 11 (2021) 16688–16697.
[4] S. Yang, K.-F. Leong, Z. Du, C.-K. Chua, The design of scaffolds for use in tissue engineering. Part I. Traditional factors, Tissue Eng. 7 (2001) 679–689.
[5] F.R. Maia, A.R. Bastos, J.M. Oliveira, V.M. Correlo, R.L. Reis, Recent approaches towards bone tissue engineering, Bone 154 (2022) 116256.
[6] C. Wen, Y. Yamada, K. Shimojima, Y. Chino, H. Hosokawa, M. Mabuchi, Novel titanium foam for bone tissue engineering, J. Mater. Res. 17 (2002) 2633–2639.
[7] J.D. Oliveira, P.D. Aguiar, A. Rossi, G. Soares, Effect of process parameters on the characteristics of porous calcium phosphate ceramics for bone tissue scaffolds, Artif. Organs 27 (2003) 406–411.
[8] J. Xiong, Y. Li, P.D. Hodgson, Ce Wen, Influence of porosity on shape memory behavior of porous TiNi shape memory alloy, Funct. Mater. Lett. 1 (2008) 215–219.
[9] T. Vos, C. Allen, M. Arora, R.M. Barber, Z.A. Bhutta, A. Brown, A. Carter, D.C. Casey, F.J. Charlson, A.Z. Chen, Global, regional, and national incidence, prevalence, and years lived with disability for 310 diseases and injuries, 1990–2015: a systematic analysis for the Global Burden of Disease Study 2015, lancet 388 (2016) 1545–1602.
[10] D.N. Wolman, J.J. Heit, Recent advances in vertebral augmentation for the treatment of vertebral body compression fractures, Curr. Phys. Med. Rehabil. Rep. 5 (2017) 161–174.
[11] N.S. Morozova, D.A. Kolbovsky, A.I. Kazmin, S.V. Kolesov, The use of nitinol rods in surgical treatment of degenerative scoliosis. 2.5-year follow-up, Coluna/Column. 15 (2016) 22–25.
[12] K. Khanlari, Q. Shi, X. Yan, K. Hu, C. Tan, P. Kelly, W. Zhang, P. Cao, X. Wang, X. Liu, Printing of NiTinol parts with characteristics respecting the general microstructural, compositional and mechanical requirements of bone replacement implants, Mater. Sci. Eng.: A 839 (2022) 142839.
[13] E.M. Greenfield, Anabolic effects of intermittent PTH on osteoblasts, Curr. Mol. Pharmacol. 5 (2012) 127–134.
[14] D. Kok, R. Donk, F. Wapstra, A. Veldhuizen, The memory metal minimal access cage: a new concept in lumbar interbody fusion—a prospective, noncomparative study to evaluate the safety and performance, Adv. Orthop. 2012 (2012).
[15] J. Litak, M. Szymoniuk, W. Czyżewski, Z. Hoffman, J. Litak, L. Sakwa, P. Kamieniak, Metallic implants used in lumbar interbody fusion, Materials 15 (2022) 3650.
[16] D. Kok, P.J. Firkins, F.H. Wapstra, A.G. Veldhuizen, A new lumbar posterior fixation system, the memory metal spinal system: an in-vitro mechanical evaluation, BMC Musculoskelet. Disord. 14 (2013) 1–8.
[17] D. Tahal, K. Madhavan, L.O. Chieng, G.M. Ghobrial, M.Y. Wang, Metals in spine, World Neurosurg. 100 (2017) 619–627.
[18] B. Chen, Y.-H. Zheng, T. Zheng, C.-H. Sun, J. Lu, P. Cao, J.-H. Zhou, The implantation of a Nickel-Titanium shape memory alloy ameliorates vertebral body compression fractures: a cadaveric study, Int. J. Clin. Exp. Med. 8 (2015) 16899.
[19] K. Otsuka, X. Ren, Physical metallurgy of Ti–Ni-based shape memory alloys, Prog. Mater. Sci. 50 (2005) 511–678.
[20] L. Machado, M. Savi, Medical applications of shape memory alloys, Braz. J. Med. Biol. Res. 36 (2003) 683–691.
[21] R. Chaudhari, J.J. Vora, D. Parikh, A review on applications of nitinol shape memory alloy, Recent Adv. Mech. Infrastruct. (2021) 123–132.
[22] R.A. Ayers, S.J. Simske, T. Bateman, A. Petkus, R. Sachdeva, V. Gyunter, Effect of nitinol implant porosity on cranial bone ingrowth and apposition after 6 weeks, J. Biomed. Mater. Res.: Off. J. Soc. Biomater. Jpn. Soc. Biomater. Aust. Soc. Biomater. 45 (1999) 42–47.
[23] E. Topolnitskiy, T. Chekalkin, E. Marchenko, Y. Yasenchuk, J.-h Kang, L.H. Yahia, Combination of Solid and Porous Nitinol Implants in Surgical Treatment of Extensive Post-Excision Thoracic Defects in Cancer Patients, SMST2022, ASM International, 2022, pp. 79–80.
[24] M. Ghanbari, M. Salavati-Niasari, F. Mohandes, Nanocomposite scaffolds based on gelatin and alginate reinforced by Zn2SiO4 with enhanced mechanical and chemical properties for Tissue Engineering, Arab. J. Chem. (2022) 103730.
[25] A. Oyane, H.M. Kim, T. Furuya, T. Kokubo, T. Miyazaki, T. Nakamura, Preparation and assessment of revised simulated body fluids, J. Biomed. Mater. Res. Part A: Off. J. Soc. Biomater., Jpn. Soc. Biomater., Aust. Soc. Biomater. Korean Soc. Biomater. 65 (2003) 188–195.
[26] M. Ghanbari, M. Salavati-Niasari, F. Mohandes, Injectable hydrogels based on oxidized alginate-gelatin reinforced by carbon nitride quantum dots for tissue engineering, Int. J. Pharm. 602 (2021) 120660.
[27] R. Singh, A.K. Sharma, A.K. Sharma, Physical and mechanical behavior of NiTi composite fabricated by newly developed uni-axial compaction die, Mater. Res. 24 (2021).
[28] A. Pasturel, C. Colinet, D.N. Manh, A. Paxton, M. Van Schilfgaarde, Electronic structure and phase stability study in the Ni-Ti system, Phys. Rev. B 52 (1995) 15176.
[29] P. Villars, L. Calvert, Pearson's Handbook of Crystallographic Data for Intermediate Phases, American Society of Metals, Cleveland, OH, 1985.
[30] S. Zhu, X. Yang, D. Fu, L. Zhang, C. Li, Z. Cui, Stress–strain behavior of porous NiTi alloys prepared by powders sintering, Mater. Sci. Eng.: A 408 (2005) 264–268.
[31] M. Mehrpouya, A. Gisario, M. Elahinia, Laser welding of NiTi shape memory alloy: a review, J. Manuf. Process. 31 (2018) 162–186.
[32] S. Sadrnezhaad, M. Parsafar, Y. Rashtiani, M. Jadidi, Nitinol spinal vertebrae: a favorable new substitute, Int. J. Eng. 32 (2019) 842–851.
[33] N. Sharma, K.K. Jangra, T. Raj, Fabrication of NiTi alloy: a review, Proc. Inst. Mech. Eng., Part L: J. Mater.: Des. Appl. 232 (2018) 250–269.
[34] L. Tao, J.-l XU, Q.-f XIAO, Y.-x TONG, J. HUANG, J.-p ZHANG, J.-m LUO, L. Yong, Preparation and characterization of porous NiTi alloys synthesized by microwave sintering using Mg space holder, Trans. Nonferrous Met. Soc. China 31 (2021) 485–498.
[35] C. Chu, C. Chung, P. Lin, S. Wang, Fabrication of porous NiTi shape memory alloy for hard tissue implants by combustion synthesis, Mater. Sci. Eng.: A 366 (2004) 114–119.
[36] E. Sgambitterra, P. Magaro, F. Niccoli, F. Furgiuele, C. Maletta, Fatigue crack growth in austenitic and martensitic NiTi: modeling and experiments, Shape Mem. Superelasticity 7 (2021) 250–261.
[37] Z. Guan, J. Bai, J. Gu, X. Liang, D. Liu, X. Jiang, R. Huang, Y. Zhang, C. Esling, X. Zhao, First-principles investigation of B2 partial disordered structure, martensitic transformation, elastic and magnetic properties of all-d-metal Ni-Mn-Ti Heusler alloys, J. Mater. Sci. Technol. 68 (2021) 103–111.
[38] Y. Sun, Y. Zhao, H. Zhang, Y. Rong, R. Yao, Y. Zhang, X. Yao, R. Hang, Corrosion behavior, antibacterial ability, and osteogenic activity of Zn-incorporated Ni-Ti-O nanopore layers on NiTi alloy, J. Mater. Sci. Technol. 97 (2022) 69–78.
[39] S. Singh, A. Jinoop, I. Palani, C. Paul, K. Tomar, K. Prashanth, Microstructure and mechanical properties of NiTi-SS bimetallic structures built using Wire Arc Additive Manufacturing, Mater. Lett. 303 (2021) 130499.